

Analytical form of the particle distribution based on the cumulant solution of the elastic Boltzmann transport equation

W. Cai, M. Xu, and R. R. Alfano

Institute for Ultrafast Spectroscopy and Lasers, New York State Center of Advanced Technology for Ultrafast Photonic Materials and Applications, Department of Physics, The City College and Graduate Center of City University of New York, New York, New York 10031, USA

(Received 17 November 2004; revised manuscript received 2 February 2005; published 5 April 2005)

An analytical expression of the particle distribution based on an analytical cumulant solution of the time-dependent elastic Boltzmann transport equation (BTE) is presented. This expression improves upon the previous second order cumulant solution of the BTE described by a Gaussian distribution in two aspects: (1) separating the ballistic component from the scattered component to ensure that the summation in expressions is convergent; and (2) enforcing the causality condition to ensure that no particle travels faster than the free speed of the particles. Time-resolved profiles obtained using the analytical form are compared with those obtained by the Monte Carlo simulation, for both transmission and backscattering. The calculating time using our analytical form is much faster than that using the Monte Carlo approach.

DOI: 10.1103/PhysRevE.71.041202

PACS number(s): 42.25.Dd, 05.60.Cd, 05.20.-y, 42.25.Fx

I. INTRODUCTION

The time-dependent elastic Boltzmann transport equation (BTE) describes the particle (and light, acoustic wave, etc.) propagation with time in a scattering medium, where the particles suffer multiple scattering by randomly distributed scatterers. The BTE is also called the radiative transfer equation in light propagation [1–3]. The solutions of the elastic BTE are applied in broad areas, such as atmospheric science, medical imaging, and solid state physics.

An example is the approach to optical imaging of human tissue that is often called “diffusion tomography,” because the theoretical model is built based on the solution of the diffusion equation. The diffusion equation is the lowest order approximation of the radiative transfer equation, which has significant error when the distance between a voxel and a source is short. However, the contribution from these voxels near the source to the measured signals is much larger than that from voxels deep inside body. Hence, for accurate imaging the theoretical model should be based on solution of the radiative transfer equation. A similar procedure can be applied to images of cloud distribution obtained using a lidar arranged on a satellite, which requires knowledge of the multiple scattering effect of water drops distributed in the cloud on the time-resolved backscattering signals. In both examples, the size of the scatterers can be nearly equal to or larger than the wavelength of light, leading to a large anisotropic factor. The use of low-frequency sound to detect oil-bearing layers deep under the ocean floor is another example.

Currently, numerical approaches, including Monte Carlo simulations, are the main methods in solving the BTE [4–6]. Numerical solution of the BTE is a cumbersome task, since the particle distribution $I(\mathbf{r}, \mathbf{s}, t)$ is a function of position \mathbf{r} , angle \mathbf{s} , and time t , in a six-dimensional space of parameters. An analytical expression for $I(\mathbf{r}, \mathbf{s}, t)$ with quantitative accuracy can greatly reduce the computation burden in modeling particle and light propagation in scattering media, which is essential for imaging in turbid media, because the inverse

reconstruction process calls the forward model many times.

Recently, we have developed an analytical solution of the time-dependent elastic BTE in an infinite uniform medium with an arbitrary phase function [7,8]. The exact spatial cumulants of $I(\mathbf{r}, \mathbf{s}, t)$ up to an arbitrary high order at any angle and any time have been derived. A cutoff at second order of the cumulants $I(\mathbf{r}, \mathbf{s}, t)$ can be approximately expressed by a Gaussian distribution, which has the exact first cumulant (the position of the center of the distribution) and the exact second cumulant (the half-width of the spread of the distribution). The cumulant solution of BTE has been extended to the case of a polarized photon distribution, and to semi-infinite and slab geometries. Using a perturbation method, the distribution $I(\mathbf{r}, \mathbf{s}, t)$ in a weak heterogeneous medium can be calculated based on the cumulant solution of the BTE.

The analytical cumulant solution of the BTE obtained, although it has exact center and half-width, is not satisfactory in two respects. First, one cannot ensure that the summation over l in the expressions shown in Sec. II is convergent at very early times. Second, a remarkable fault of the Gaussian distribution at early times is that particles at the front edge of the distribution travel faster than the free speed of the particles in the medium, thus violating causality, especially for those particles moving along near forward directions. The Gaussian distribution is accurate at long times and in the backscattering case, since many collisions lead to a Gaussian distribution according to the central limit theorem.

In this paper, the analytical cumulant solution of the BTE has been improved compared to our previous work [7] in these two respects. For solving the first problem, we make a separation of the ballistic component from the total $I(\mathbf{r}, \mathbf{s}, t)$ and compute the cumulants for the scattered component $I^{(s)}(\mathbf{r}, \mathbf{s}, t)$. This treatment ensures convergent summation over l . Also this separation provides a clearer picture of particle propagation. In the time-resolved transmission profile the ballistic component is described by a sharp jump exactly at the ballistic time, separated from the later scattered component. For solving the second problem two approaches are

used. The first method is to calculate the distribution including the higher-order cumulants, based on our work in Ref. [8]. However, computation of high-order cumulants is a cumbersome task. In the second method the Gaussian distribution is replaced by a different-shaped form, which satisfies causality, and maintains the correct center position and the correct half-width of the distribution computed by our analytical approach. There are infinite choices of the shapes of the distribution satisfying these conditions; we choose a simple analytical form. At long times, the reshaped distribution tends to the Gaussian distribution. Our results show that the reshaped distribution matches that obtained using Monte Carlo simulation much better than the Gaussian distribution.

The paper is organized as follows. In Sec. II we briefly review the main results of the analytical cumulant solution of the BTE. Section III presents a separation of the ballistic component from the scattered component, which makes the summation over l convergent. Section IV improves the distribution at early times using two approaches, and presents the numerical result compared with the Monte Carlo simulation. Section V is devoted to discussion and conclusions.

II. THE ANALYTICAL CUMULANT SOLUTION OF THE BTE

The elastic Boltzmann kinetic equation of particles, with magnitude of velocity v , for the distribution function $I(\mathbf{r}, \mathbf{s}, t)$ as a function of time t , position \mathbf{r} , and direction \mathbf{s} , in an infinite uniform medium, from a point pulse light source, $\delta(\mathbf{r}-\mathbf{r}_0)\delta(\mathbf{s}-\mathbf{s}_0)\delta(t-t_0)$, is given by

$$\begin{aligned} & \partial I(\mathbf{r}, \mathbf{s}, t) / \partial t + v \mathbf{s} \cdot \nabla_{\mathbf{r}} I(\mathbf{r}, \mathbf{s}, t) + \mu_a I(\mathbf{r}, \mathbf{s}, t) \\ &= \mu_s \int P(\mathbf{s}, \mathbf{s}') I(\mathbf{r}, \mathbf{s}', t) d\mathbf{s}' - \mu_s I(\mathbf{r}, \mathbf{s}, t) \\ &+ \delta(\mathbf{r}-\mathbf{r}_0)\delta(\mathbf{s}-\mathbf{s}_0)\delta(t-t_0) \end{aligned} \quad (1)$$

where μ_s is the scattering rate, μ_a is the absorption rate, and $P(\mathbf{s}, \mathbf{s}')$ is the phase function, normalized to $\int P(\mathbf{s}, \mathbf{s}') d\mathbf{s}' = 1$. The phase function is assumed to depend only on the scattering angle in an isotropic medium. Under this assumption, an arbitrary phase function can be handled. We expand the phase function in Legendre polynomials with constant coefficients,

$$P(\mathbf{s}, \mathbf{s}') = \frac{1}{4\pi} \sum_l a_l P_l(\mathbf{s} \cdot \mathbf{s}'). \quad (2)$$

Recently, we have developed a different approach to obtain an analytical solution of the BTE in an infinite uniform medium, based on a cumulant expansion [7,8].

We briefly review the concept of the ‘‘cumulant’’ in a one-dimensional (1D) case. Consider a random variable x , with a probability distribution function $f(x)$. Instead of using $f(x)$ to describe the distribution, we define the n th moment of x ,

$$\langle x^n \rangle = \int x^n f(x) dx, \quad (3)$$

and correspondingly the n th cumulant $\langle x^n \rangle_c$ defined by

$$\exp\left(\sum_{n=1}^{\infty} \langle x^n \rangle_c (it)^n / n!\right) = \langle \exp(itx) \rangle = \sum_{n=0}^{\infty} \langle x^n \rangle (it)^n / n! \quad (4)$$

The first cumulant $\langle x \rangle_c$ is the mean position of x . The second cumulant $\langle x^2 \rangle_c$ represents the half-width of the distribution. The higher cumulants are related to the detailed shape of the distribution. For example, $\langle x^3 \rangle_c$ describes the skewness or asymmetry of the distribution, and $\langle x^4 \rangle_c$ describes the ‘‘kurtosis’’ of the distribution, that is, the extent to which it differs from the standard bell shape associated with the Gaussian distribution function. The cumulants hence describe the distribution in an intrinsic way by subtracting off the effects of all lower-order moments. In the 3D case, the first cumulant has three components, the second cumulant has six components, and so on.

We have derived an explicit algebraic expression for the spatial cumulants at any angle and any time, exact up to an arbitrarily high order n [8]. This means the distribution function $I(\mathbf{r}, \mathbf{s}, t)$ can be computed to any desired accuracy. At the second order, $n=2$, an analytic explicit expression for distribution function $I(\mathbf{r}, \mathbf{s}, t)$ is obtained [7,8]. This distribution is Gaussian in position, which is accurate at later times, but only provides the exact mean position and the exact half-width at early times.

The Gaussian distribution of the second-order cumulant solution is written as

$$\begin{aligned} I(\mathbf{r}, \mathbf{s}, t) &= \frac{F(\mathbf{s}, \mathbf{s}_0, t)}{(4\pi)^{3/2} (\det B)^{1/2}} \\ &\times \exp\left[-\frac{1}{4} (B^{-1})_{\alpha\beta} (r-r^c)_{\alpha} (r-r^c)_{\beta}\right], \end{aligned} \quad (5)$$

where $F(\mathbf{s}, \mathbf{s}_0, t)$ is the total angular distribution $F(\mathbf{s}, \mathbf{s}_0, t) = \int I(\mathbf{r}, \mathbf{s}, t) d\mathbf{r}$, which has the following exact expression:

$$\begin{aligned} F(\mathbf{s}, \mathbf{s}_0, t) &= \exp(-\mu_a t) \sum_l \frac{2l+1}{4\pi} \exp(-g_l t) P_l(\mathbf{s} \cdot \mathbf{s}_0) \\ &= \exp(-\mu_a t) \sum_l \frac{2l+1}{4\pi} \exp(-g_l t) \sum_m Y_{lm}(\mathbf{s}) Y_{lm}^*(\mathbf{s}_0), \end{aligned} \quad (6)$$

where

$$g_l = \mu_s [1 - a_l / (2l+1)]. \quad (7)$$

Two special values of g_l are $g_0=0$, which follows from the normalization of $P(\mathbf{s}, \mathbf{s}')$, and $g_1=v/l_{tr}$, where l_{tr} is the transport mean free path, defined by $l_{tr}=v/[\mu_s(1-\langle \cos \theta \rangle)]$, where $\langle \cos \theta \rangle$ is the average of $\mathbf{s} \cdot \mathbf{s}'$ with $P(\mathbf{s}, \mathbf{s}')$ as weight. In Eq. (6), $Y_{lm}(\mathbf{s})$ are spherical harmonics normalized to $4\pi/(2l+1)$.

The center of the packet (the first cumulant), denoted by \mathbf{r}^c , is located at

$$\mathbf{r}_z^c = G \sum_l A_l P_l(\cos \theta) [(l+1)f(g_l - g_{l+1}) + lf(g_l - g_{l-1})], \quad (8)$$

$$r_x^c = G \sum_l A_l P_l^{(1)}(\cos \theta) \cos \phi [f(g_l - g_{l-1}) - f(g_l - g_{l+1})], \quad (9)$$

where $G = v \exp(-\mu_a t) / F(\mathbf{s}, \mathbf{s}_0, t)$, $A_l = (1/4\pi) \exp(-g_l t)$, and for any variable x ,

$$f(x) = [\exp(xt) - 1]/x. \quad (10)$$

r_y^c is obtained by replacing $\cos \phi$ in Eq. (9) by $\sin \phi$. In Eqs. (8) and (9), $P_l^{(m)}(\cos \theta)$ is the associated Legendre function.

The square of the average spread half-width (the second cumulant) is given by

$$B_{\alpha\beta} = vG \Delta_{\alpha\beta} - r_\alpha^c r_\beta^c / 2, \quad (11)$$

where all the coefficients are functions of angle and time:

$$\Delta_{zz} = \sum_l A_l P_l(\cos \theta) \left[\frac{l(l-1)}{2l-1} E_l^{(1)} + \frac{(l+1)(l+2)}{2l+3} E_l^{(2)} + \frac{l^2}{2l-1} E_l^{(3)} + \frac{(l+1)^2}{2l+3} E_l^{(4)} \right], \quad (12)$$

$$\begin{aligned} \Delta_{xx,yy} &= \sum_l \frac{1}{2} A_l P_l(\cos \theta) \left[-\frac{l(l-1)}{2l-1} E_l^{(1)} - \frac{(l+1)(l+2)}{2l+3} E_l^{(2)} + \frac{l(l-1)}{2l-1} E_l^{(3)} + \frac{(l+1)(l+2)}{2l+3} E_l^{(4)} \right] \\ &\pm \sum_l \frac{1}{2} A_l P_l^{(2)}(\cos \theta) \cos(2\phi) \\ &\times \left[\frac{1}{2l-1} E_l^{(1)} + \frac{1}{2l+3} E_l^{(2)} - \frac{1}{2l-1} E_l^{(3)} - \frac{1}{2l+3} E_l^{(4)} \right], \end{aligned} \quad (13)$$

where (+) corresponds to Δ_{xx} and (-) corresponds to Δ_{yy} ,

$$\Delta_{xy} = \Delta_{yx} = \sum_l \frac{1}{2} A_l P_l^{(2)}(\cos \theta) \sin(2\phi) \left[\frac{1}{2l-1} E_l^{(1)} + \frac{1}{2l+3} E_l^{(2)} - \frac{1}{2l-1} E_l^{(3)} - \frac{1}{2l+3} E_l^{(4)} \right], \quad (14)$$

$$\Delta_{xz} = \Delta_{zx} = \sum_l \frac{1}{2} A_l P_l^{(1)}(\cos \theta) \cos \phi \left[\frac{2(l-1)}{2l-1} E_l^{(1)} - \frac{2(l+2)}{2l+3} E_l^{(2)} + \frac{1}{2l-1} E_l^{(3)} + \frac{1}{2l+3} E_l^{(4)} \right]. \quad (15)$$

Δ_{yz} is obtained by replacing $\cos \phi$ in Eq. (15) by $\sin \phi$. In Eqs. (12)–(15) $E_l^{(1-4)}$ are given by

$$E_l^{(1)} = [f(g_l - g_{l-2}) - f(g_l - g_{l-1})] / (g_{l-1} - g_{l-2}), \quad (16)$$

$$E_l^{(2)} = [f(g_l - g_{l+2}) - f(g_l - g_{l+1})] / (g_{l+1} - g_{l+2}), \quad (17)$$

$$E_l^{(3)} = [f(g_l - g_{l-1}) - t] / (g_l - g_{l-1}), \quad (18)$$

$$E_l^{(4)} = [f(g_l - g_{l+1}) - t] / (g_l - g_{l+1}). \quad (19)$$

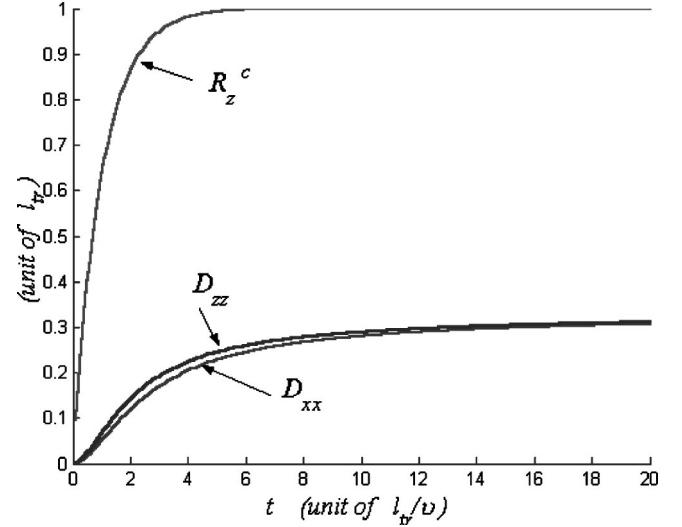


FIG. 1. The moving center R_z^c and the diffusion coefficients D_{zz} and D_{xx} of the particle density function as functions of time t .

The second order cumulant approximation for the particle density distribution $N(\mathbf{r}, t)$ has a Gaussian shape:

$$\begin{aligned} N(\mathbf{r}, t) &= \frac{1}{(4\pi D_{zz} vt)^{1/2}} \frac{1}{4\pi D_{xx} vt} \exp \left[-\frac{(z - R_z^c)^2}{4D_{zz} vt} \right] \\ &\times \exp \left[-\frac{(x^2 + y^2)}{4D_{xx} vt} \right] \exp(-\mu_a t), \end{aligned} \quad (20)$$

with a moving center located at

$$R_z^c = v[1 - \exp(-g_1 t)] / g_1, \quad (21)$$

and the corresponding time-dependent diffusion coefficients are given by

$$\begin{aligned} D_{zz} &= \frac{v}{3t} \left\{ \frac{t}{g_1} - \frac{3g_1 - g_2}{g_1^2(g_1 - g_2)} [1 - \exp(-g_1 t)] \right. \\ &\left. + \frac{2}{g_2(g_1 - g_2)} [1 - \exp(-g_2 t)] - \frac{3}{2g_1^2} [1 - \exp(-g_1 t)]^2 \right\}, \end{aligned} \quad (22)$$

$$\begin{aligned} D_{xx} = D_{yy} &= \frac{v}{3t} \left\{ \frac{t}{g_1} + \frac{g_2}{g_1^2(g_1 - g_2)} [1 - \exp(-g_1 t)] \right. \\ &\left. - \frac{1}{g_2(g_1 - g_2)} [1 - \exp(-g_2 t)] \right\}. \end{aligned} \quad (23)$$

Each distribution in Eqs. (5) and (20) describes a particle “cloud” anisotropically spreading from a moving center, with time-dependent diffusion coefficients. As shown in Fig. 1, at early time $t \rightarrow 0$, the mean position of the photons moves along the \mathbf{s}_0 direction with speed v , and the diffusion coefficient tends to zero. These results present a clear picture of nearly ballistic motion at $t \rightarrow 0$. With increase of time, the motion of the center slows down, and the diffusion coefficients increase from zero. This stage of particle migration is often called a “snakelike mode.” At late times, the total angular distribution function tends to become isotropic. The

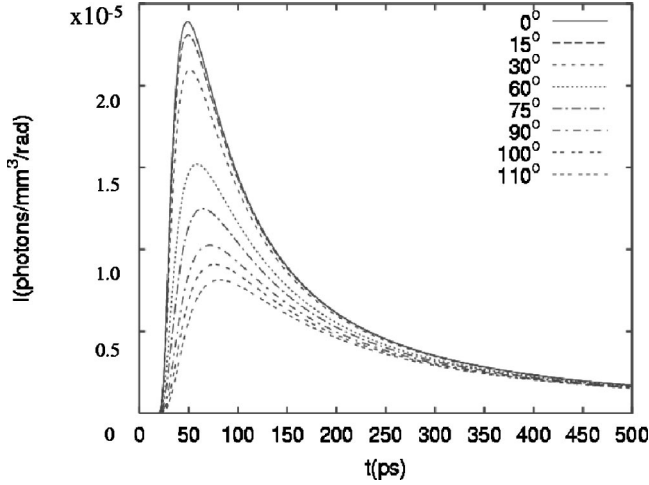


FIG. 2. Light distribution in an infinite uniform medium as a function of time at different received angles, using the second cumulant solution of the BTE (Gaussian distribution), where the detector is located at $z=10$ mm from the source in the incident direction. The parameters for this calculation are $l_{tr}=2$ mm, the absorption length $l_a=300$ mm, the phase function is computed using Mie theory for polystyrene spheres with diameter $d=1.11$ μm in water, and the wavelength of the laser source $\lambda=625$ nm, which gives the g factor $g=0.926$.

particle density, at $t \gg l_{tr}/v$ and $r \gg l_{tr}$, tends toward the center-moved ($1/l_{tr}$) diffusion solution with the diffusive coefficient $l_{tr}/3$. Therefore, our solution quantitatively describes how particles migrate from nearly ballistic motion, to snakelike motion, and then to diffusive motion.

Figure 2 shows the calculated distribution as a function of time at different receiving angles in an infinite uniform medium, computed by the second order cumulant solution, where the detector is located at $5l_{tr}$ from the source in the incident direction of the source. Figure 2 shows anisotropy of the distribution at a distance of $5l_{tr}$ from the source. This type of distribution has been demonstrated by time-resolved experiments [9].

The analytical solution obtained, although it has the exact center and half-width, is not satisfactory in two respects. First, at very early times, $\exp(-gt) \rightarrow 1$ for all l ; hence, one cannot ensure that summation over l is convergent. Second, particles at the front edge of the Gaussian distribution travel faster than the speed v , thus violating causality.

III. SEPARATING THE BALLISTIC COMPONENT FROM THE SCATTERED COMPONENT

In order to make the summation over l convergent, we separate the ballistic component from the total $I(\mathbf{r}, \mathbf{s}, t)$, and compute the cumulants for the scattered component $I^{(s)}(\mathbf{r}, \mathbf{s}, t)$.

The ballistic component is the solution of the homogeneous Boltzmann transport equation, which is the transport equation, Eq. (1), without the “scattering in” term [the first term in the right side of Eq. (1)]. The solution of the ballistic component is given by

$$I^{(b)}(\mathbf{r}, \mathbf{s}, t) = \exp[-(\mu_s + \mu_a)t] \delta(\mathbf{r} - v\mathbf{t}\mathbf{s}_0) \delta(\mathbf{s} - \mathbf{s}_0). \quad (24)$$

The moments of the ballistic component can be easily calculated. When \mathbf{s}_0 is along z , we have

$$\int z^n I^{(b)}(\mathbf{r}, \mathbf{s}, t) d^3r = \exp[-(\mu_s + \mu_a)t] (vt)^n \delta(\mathbf{s} - \mathbf{s}_0), \quad (25)$$

and other moments related to $z^{n_1} x^{n_2} y^{n_3}$ ($n_2, n_3 \neq 0$) are zero.

The total distribution is the summation of the ballistic component and the scattered component:

$$I(\mathbf{r}, \mathbf{s}, t) = I^{(b)}(\mathbf{r}, \mathbf{s}, t) + I^{(s)}(\mathbf{r}, \mathbf{s}, t); \quad (26)$$

hence, the moments of the scattered component can be obtained by subtracting the corresponding ballistic moments from the moments of $I(\mathbf{r}, \mathbf{s}, t)$. For example, we have

$$\int z^n I^{(s)}(\mathbf{r}, \mathbf{s}, t) d^3r = \int z^n I(\mathbf{r}, \mathbf{s}, t) d^3r - \int z^n I^{(b)}(\mathbf{r}, \mathbf{s}, t) d^3r. \quad (27)$$

Notice that

$$\delta(\mathbf{s} - \mathbf{s}_0) = \sum_l [(2l+1)/4\pi] P_l(\mathbf{s} \cdot \mathbf{s}_0). \quad (28)$$

Substituting Eqs. (25) and (28) into Eq. (27), the corresponding cumulants for the scattered component $I^{(s)}(\mathbf{r}, \mathbf{s}, t)$ can be easily obtained; they replace Eqs. (6), (8), and (12) by

$$F^{(s)}(\mathbf{s}, \mathbf{s}_0, t) = \exp(-\mu_a t) \sum_l \frac{2l+1}{4\pi} [\exp(-gt) - \exp(-\mu_s t)] P_l(\mathbf{s} \cdot \mathbf{s}_0), \quad (29)$$

$$r_z^{(s)} = G \sum_l P_l(\cos \theta) \frac{1}{4\pi} \{ \exp(-gt) [(l+1)f(g_l - g_{l+1}) + lf(g_l - g_{l-1})] - (2l+1)t \exp(-\mu_s t) \}, \quad (30)$$

$$\Delta_{zz}^{(s)} = \sum_l P_l(\cos \theta) \frac{1}{4\pi} \left\{ \exp(-gt) \left[\frac{l(l-1)}{2l-1} E_l^{(1)} + \frac{(l+1)(l+2)}{2l+3} E_l^{(2)} + \frac{l^2}{2l-1} E_l^{(3)} + \frac{(l+1)^2}{2l+3} E_l^{(4)} \right] - \frac{t^2(2l+1)}{2} \exp(-\mu_s t) \right\}. \quad (31)$$

The expressions for the other components of the first and second cumulants are unchanged, provided all $F(\mathbf{s}, \mathbf{s}_0, t)$ in Sec. II are replaced by $F^{(s)}(\mathbf{s}, \mathbf{s}_0, t)$. Note that Eq. (28) actually is equal to zero at $\mathbf{s} \neq \mathbf{s}_0$, and there is no ballistic component in these directions.

The replacement of equations in Sec. II by Eqs. (29)–(31) greatly improves the calculation of cumulants at very early times. By the subtraction introduced above, the terms for large l approach zero, and summation over l becomes convergent at very early times. When $t \rightarrow 0$, $g_l = \mu_s [1 - a_l / (2l+1)]$ [see Eq. (7)] approaches μ_s for large l , $f(g_l - g_{l\pm 1}) \approx t$

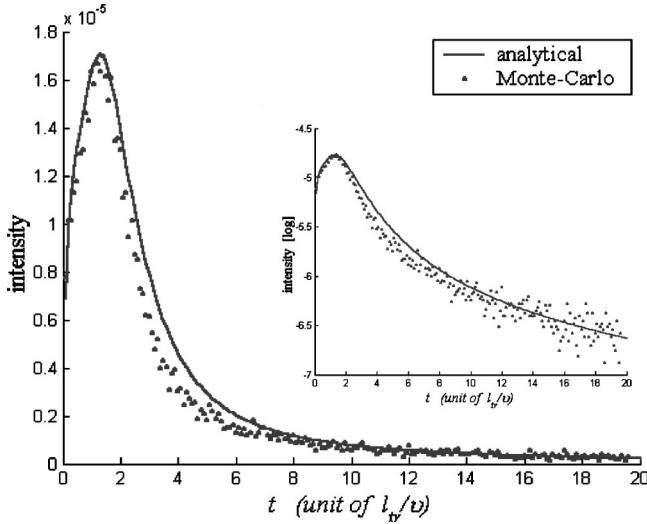


FIG. 3. Time-resolved profile of the backscattered (180°) photon intensity inside a disk with center at $\mathbf{r}=\mathbf{0}$, radius $R=1l_{tr}$, thickness $dz=0.1l_{tr}$, and the received solid angle $d\cos\theta=0.001$, normalized to inject one photon. The Heyney-Greenstein phase function with $g=0.9$ is used, and $1/l_a=0$. The solid curve is for the second cumulant solution (Gaussian distribution), and dots are for the Monte Carlo simulation. The inset diagram shows the same result drawn using a logarithmic scale for intensity.

[see Eq. (10)], and $E_l^{(1-4)} \approx t^2/2$ [see Eqs. (16)–(19)], which results in cancellation in the summand for large l at very early times.

An example of successful use of this replacement is the calculation of backscattering. When $\theta=180^\circ$, $P_l(\cos\theta)=1$ or -1 , depending on whether l is even or odd. The computed r_z^c at very early times using Eq. (8) oscillates with a cutoff of \bar{l} . But the computed $r_z^{c(s)}$ at very early times using Eq. (30) becomes stable. Calculation shows that $r_z^{c(s)}=0$ at any time when $\theta=180^\circ$.

Figure 3 shows the computed time profile of the backscattering intensity $I^{(s)}(\mathbf{r}, \mathbf{s}, t)$ at a detector centering at $\mathbf{r}=\mathbf{0}$ and received at an angle $\theta=180^\circ$, which actually is the total backscattering intensity $I(\mathbf{r}, \mathbf{s}, t)$ because $\mathbf{s} \neq \mathbf{s}_0$, compared with the Monte Carlo simulation. The absolute value of the intensity, as well as the shape of the time-resolved profile, computed using our analytical cumulant solution of the BTE match well with those of the Monte Carlo simulation. The inset diagram is the same result drawn using a logarithmic scale for intensity. Note that this result of backscattering, based on the solution of the BTE, is for a detector located near the source, different from other backscattering results based on the diffusion model, which is only valid when detector is located at a distance of several l_{tr} from the source.

IV. SHAPE OF THE PARTICLE DISTRIBUTION

If the cumulants with order $n>2$ are assumed all zero, the distribution becomes Gaussian. The Gaussian distribution is accurate at long times. At early times, particles at the front edge of the distribution travel faster than the free speed of the particles, thus violating causality, especially for particles

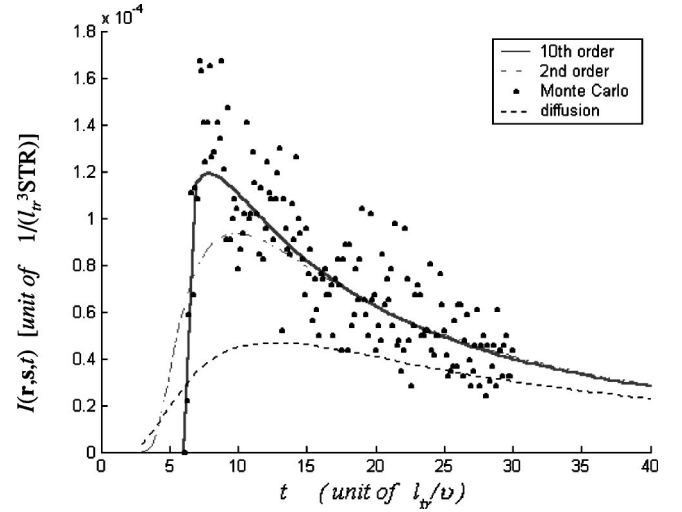


FIG. 4. Time-resolved profile of transmitted light in an infinite uniform medium, computed using the tenth order cumulant solution (solid curve), the second order cumulant solution (dotted curve), and the diffusion approximation (thick dots curve), compared with that of the Monte Carlo simulation (discrete dots). The detector is located at $z=6l_{tr}$ from the source along the incident direction, and the received direction is $\theta=0$. The Heyney-Greenstein phase function with $g=0.9$ is used, and the absorption coefficient $1/l_a=0$.

that move along near forward directions. In the following, two approaches are used for overcoming this fault: (A) including higher cumulants; and (B) introducing a reshaped distribution.

A. Calculation including high-order cumulants

We have performed calculations including the higher-order cumulants to obtain a more accurate shape of the distribution. The Codes for calculation are designed based on a formula derived in Ref. [8].

Figure 4 shows $I(\mathbf{r}, \mathbf{s}, t)$ with the detector located at $z=6l_{tr}$ in front of the source and receiving direction along $\theta=0$, computed using the analytical cumulant solution up to tenth order of the cumulants (solid curve), up to the second order cumulants (dotted curve), in the diffusion approximation (thick dotted curve), and the Monte Carlo simulation (discrete dots). The figure shows that the tenth order cumulant solution is located in the middle of the data obtained by the Monte Carlo simulation, and $I(\mathbf{r}, \mathbf{s}, t) \approx 0$ before the ballistic time $t_b=6l_{tr}/v$. The second order cumulant solution has nonzero $I(\mathbf{r}, \mathbf{s}, t)$ before t_b , which violates causality. The computed $N(\mathbf{r}, t)/4\pi$ using the diffusion model has a large discrepancy with the Monte Carlo simulation, and the diffusion solution has more nonzero components before t_b , which violates causality.

Using the second order cumulant solution, the distribution function can be computed very fast. The associated Legendre functions can be quickly computed using recurrence relations with accuracy limited by the computer machine error. It takes 1 min to produce 10^5 data points of $I(\mathbf{r}, \mathbf{s}, t)$ on a personal computer. On the other hand, in order to reduce the statistical fluctuation to the level shown in Fig. 4, 10^9 events

are counted in the Monte Carlo simulation, which takes tens of hours computation time on a personal computer. Computation of high-order cumulants also is a cumbersome task, because the number of involved terms rapidly grows with increase of the order n . Also, for a distribution function that is positive definite, the Bust theorem states that the existence of nonzero cumulants of any order higher than 2 will be accompanied by nonzero cumulants of all orders [10]. Therefore, no matter how the cutoff at a finite high order n is taken, the cumulant solution of the BTE cannot be regarded as exact.

B. Reshaping the particle distribution

For practical applications, we use a semiphenomenological model. The Gaussian distribution is replaced by a different-shaped form, which maintains the correct center position and the correct half-width of the distribution. This distribution satisfies causality, namely, $I(\mathbf{r}, \mathbf{s}, t) = 0$ outside the ballistic limit vt . There are an infinite number of choices of shape of the distribution under the above conditions. We choose a simple analytical form as discussed later. At long times, the half-width of the distribution $\sigma \sim (4B)^{1/2}$, with B shown in Eq. (11), spreads as $t^{1/2}$; hence, $\sigma \ll vt$ at large t , and the Gaussian distribution at long times with half-width σ can be regarded as completely inside the ballistic sphere. The reshaped distribution of $I(\mathbf{r}, \mathbf{s}, t)$ hence should approach the Gaussian distribution at long times.

1. 1D density

We first discuss the one-dimensional density as an example to explain our model.

The Gaussian distribution of 1D density is described by

$$N(z) = (4\pi D_{zz} vt)^{-1/2} \exp[-(z - R_z^c)^2 / (4D_{zz} vt)], \quad (32)$$

where R_z^c and D_{zz} are given in Eqs. (21) and (22). As shown in Fig. 5, although the 1D Gaussian spatial distribution (the dashed curve) at time $t = 2l_{tr}/v$, Eq. (32), has the correct center and half-width, the curve deviates from the distribution computed by the Monte Carlo simulation (dots), and a remarkable part of the distribution appears outside the ballistic limit $vt = 2l_{tr}$. At early times the spatial distribution is not symmetric about the center R^c . When R^c moves from the source toward the forward side, causality prohibits particles appearing beyond vt . This requires the particles in the forward side to be squeezed in a narrow region between R^c and vt . For a balance of the parts of the distribution in the forward and backward sides of R^c , the peak of the distribution should move to a point at the forward side and the height of the peak should increase. The earlier the time t , the closer is R^c to vt , and the asymmetry of the distribution becomes stronger. Based on this observation we propose the following analytical expression: (1) to move the peak position of the distribution from R_z^c to z_c , where the parameter z_c will be determined later; (2) to take this point as the origin of new coordinates; and (3) to use the following form of the shape of the 1D density in the new coordinates:

$$N(\tilde{z}) = b \exp(-\alpha^2 \tilde{z}^2) [1 - (\tilde{z}/\tilde{z}_\pm)^2], \quad (33)$$

where

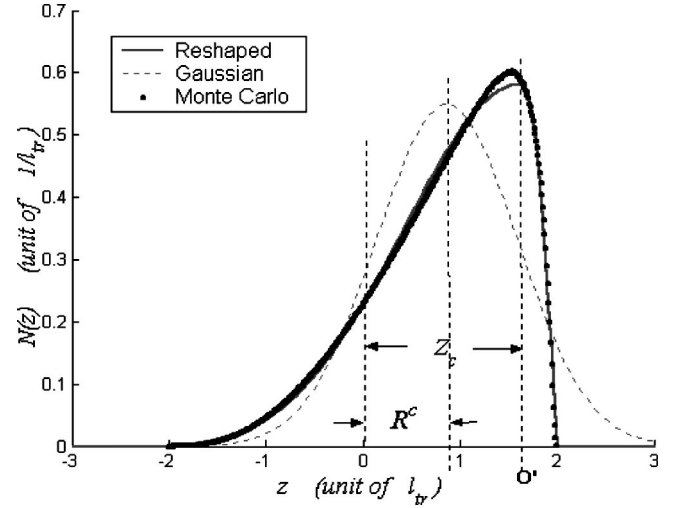


FIG. 5. The 1D spatial photon density at time $t = 2l_{tr}/v$, obtained by the reshaped form Eq. (33) (solid curve) and the Gaussian form (dashed curve), compared with that of the Monte Carlo simulation (dots). The Heyney-Greenstein phase function with $g = 0.9$ is used, and $1/l_a = 0$. In the figure, the unit on the z axis is l_{tr} ; R^c is the center position of the distribution computed by the cumulant solution; z_c is the distance between the origin of the new coordinates and the source.

$$\tilde{z}_\pm = vt \mp z_c \quad \begin{cases} \tilde{z} > 0, \\ \tilde{z} < 0. \end{cases} \quad (34)$$

At the ballistic limit $\tilde{z} = \tilde{z}_\pm$, $N(\tilde{z})$ reduces to zero, and $N(\tilde{z}) = 0$ when \tilde{z} is outside of \tilde{z}_\pm . The parameter b in Eq. (33) can be determined by normalization; the parameters (α, z_c) can be determined by fitting the center and half-width of the distribution. This fit requires

$$\int N(\tilde{z}) d\tilde{z} = 1, \quad (35)$$

$$\langle \tilde{z} \rangle = \int \tilde{z} N(\tilde{z}) d\tilde{z} = R_z^c - z_c, \quad (36)$$

$$\langle \tilde{z}^2 \rangle_c = \int (\tilde{z} - \langle \tilde{z} \rangle)^2 N(\tilde{z}) d\tilde{z} = 2D_{zz} vt. \quad (37)$$

The integrals in Eqs. (35)–(37) can be analytically performed; they are related to the standard error function (the incomplete gamma function, or the confluent hypergeometric function of the first kind):

$$F^{(0)}(\beta) = \int_0^\beta e^{-y^2} dy = \frac{\pi^{1/2}}{2} \text{erf}(\beta), \quad (38)$$

$$F^{(1)}(\beta) = \int_0^\beta e^{-y^2} y dy = \frac{1}{2} [1 - e^{-\beta^2}], \quad (39)$$

$$F^{(2n)}(\beta) = \int_0^\beta e^{-y^2} y^{2n} dy = \frac{1}{2}[(2n-1)F^{(2n-2)}(\beta) - \beta^{2n-1}e^{-\beta^2}], \quad (40)$$

$$F^{(2n+1)}(\beta) = \int_0^\beta e^{-y^2} y^{2n+1} dy = \frac{1}{2}[2nF^{(2n-1)}(\beta) - \beta^{2n}e^{-\beta^2}]. \quad (41)$$

For nonlinear fitting a difficulty is how to quickly find a global minimum. The optimization codes require setting a good initial value of the parameters, so the obtained local minimum is the true global minimum. Since we have no experience for setting good initial parameters at a special time, the following procedure is used. At the long time limit $z_c \approx R_z^c$ and $\alpha^2 \approx (4D_{zz}vt)^{-1}$, the distribution approaches the original Gaussian distribution. We make a nonlinear fitting at a point of long time t_m , using these values of the parameters as initial values. Then, we make a fitting at $t_{m-1} = t_m - \Delta t$, where Δt is a small time interval, with the initial values of parameters from those obtained at t_m , to produce parameters at t_{m-1} . Step by step, the parameters in the whole time period can be computed. Our test shows that the fitting program using this procedure runs quickly, with very small fitting error, up to a certain short time limit.

The solid curve in Fig. 5 shows the reshaped spatial distribution, Eq. (33), of 1D density at time $t = 2l_{tr}/v$, using the Heyney-Greenstein phase function with $g = 0.9$, which satisfies causality and matches the Monte Carlo result much better than the Gaussian distribution.

2. 3D density

In this case the ballistic limit is represented by a sphere with center located at the source position and the radius vt . We move the peak position of the distribution from R_z^c to z_c along the $\mathbf{s}_0 = \hat{\mathbf{z}}$ direction, take this point as the origin of new coordinates, and use the following form of the shape of the 3D density as a function of position in the new coordinates, $\tilde{\mathbf{r}}$:

$$N(\tilde{\mathbf{r}}) = b \exp[-\alpha(\tilde{\chi})^2 \tilde{r}^2][1 - (\tilde{r}/\tilde{r}^*)^2], \quad (42)$$

and $N(\tilde{\mathbf{r}}) = 0$ when $\tilde{r} > \tilde{r}^*$, where $\tilde{\chi}$ is the polar angle of $\tilde{\mathbf{r}}$ in the new coordinates, and \tilde{r}^* is the distance between the new origin and the point obtained by extrapolating $\tilde{\mathbf{r}}$ to the surface of the ballistic sphere,

$$\tilde{r}^* = [(vt)^2 - z_c^2 \sin^2(\tilde{\chi})]^{1/2} - \cos(\tilde{\chi})z_c. \quad (43)$$

In Eq. (42) $\alpha(\tilde{\chi})$ is defined by

$$\alpha(\tilde{\chi})^2 \equiv \alpha_z^2 \cos^2(\tilde{\chi}) + \alpha_\perp^2 \sin^2(\tilde{\chi}). \quad (44)$$

The parameters b can be determined by normalization; the parameters $(\alpha_z, \alpha_\perp, z_c)$ are determined by fitting the center and half-width of the distribution. This fit requires

$$\langle \tilde{z} \rangle = \int \tilde{r} \cos(\tilde{\chi}) N(\tilde{\mathbf{r}}) d^3\tilde{r} = R_z^c - z_c, \quad (45)$$

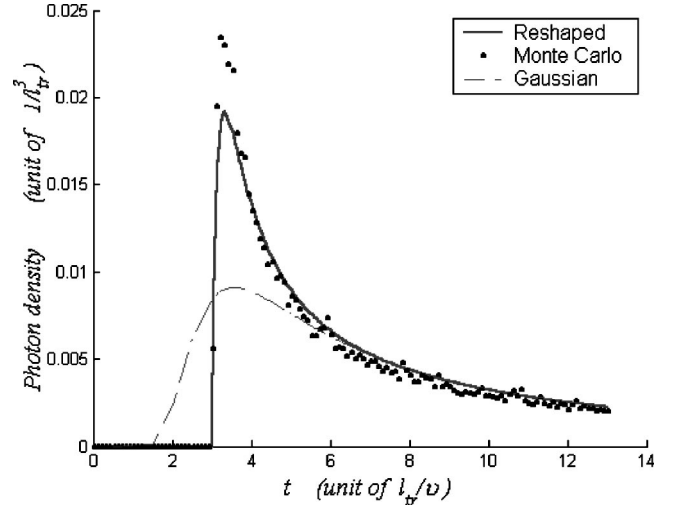


FIG. 6. Time-resolved profile of 3D photon density, where the detector is located at $z = 3l_{tr}$ from the source along the incident direction, obtained by the reshaped form Eq. (42) (solid curve) and the Gaussian form (dashed curve), compared with that of the Monte Carlo simulation (dots). The Heyney-Greenstein phase function with $g = 0.9$ is used, and the absorption coefficient $1/l_a = 0$.

$$\int [\tilde{r} \cos(\tilde{\chi}) - \langle \tilde{z} \rangle]^2 N(\tilde{\mathbf{r}}) d^3\tilde{r} = 2D_{zz}vt, \quad (46)$$

$$\int [\tilde{r} \sin(\tilde{\chi})]^2 N(\tilde{\mathbf{r}}) d^3\tilde{r} = 4D_{xx}vt. \quad (47)$$

In the above integral $d^3\tilde{r} = 2\pi\tilde{r}^2 d\tilde{r} d\cos(\tilde{\chi})$, integration over \tilde{r} can be analytically performed, and integration over $\tilde{\chi}$ is performed numerically.

Figure 6 shows the computed time profile of the 3D density $N(\mathbf{r}, t)$, with the source at the origin and the detector located at $\mathbf{r} = (0, 0, 3l_{tr})$, using the Heyney-Greenstein phase function with $g = 0.9$. The solid curve is for the reshaped form using Eq. (42). The dashed curve is for the Gaussian form, and the dots are for the Monte Carlo simulation. The results clearly demonstrate an improvement by use of the reshaped form over use of the Gaussian form. The nonzero intensity before $t_b = 3l_{tr}/v$ in the reshaped form has been completely removed, while the Gaussian distribution has nonzero components before t_b . The reshaped time profile matches with the result of the Monte Carlo simulation in most of the time period, but the peak values are about 20% lower. The errors are much smaller than those of the Gaussian distribution. By integration over time, the density for the steady state can be obtained. The difference in the steady state density between the reshaped analytical model and the Monte Carlo simulation is about 3%.

3. Distribution function $I^{(s)}(\mathbf{r}, \mathbf{s}, t)$

When the detector is located less than $8l_{tr}$ from the source in a medium with large g factor, the distribution function $I^{(s)}(\mathbf{r}, \mathbf{s}, t)$ is highly anisotropic, and the intensity received

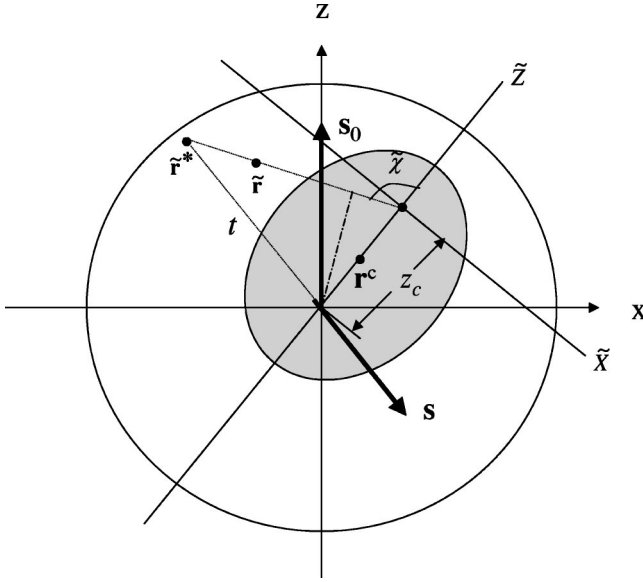


FIG. 7. Schematic diagram describing the geometry of the particle spatial distribution for scattering along a direction $\mathbf{s} \neq \mathbf{s}_0$. At a certain time t , the center of the distribution is located at \mathbf{r}^c . The half-width of the spread is characterized by an ellipsoid (the gray area). The large sphere represents the ballistic limit. The origin of the new coordinates is set by extending from $|\mathbf{r}^c|$ to z_c . $\tilde{\mathbf{r}}^*$ is the point obtained by extrapolating a position $\tilde{\mathbf{r}}$ (in the new coordinates) to the surface of the ballistic sphere, and the length \tilde{r}^* is determined by Eq. (43).

strongly depends on the angle. One needs to use the photon distribution function $I^{(s)}(\mathbf{r}, \mathbf{s}, t)$ instead of the photon density $N(\mathbf{r}, t)$.

In this case the center position \mathbf{r}^c , as a function of (\mathbf{s}, t) , is not located on the axis at incident direction \mathbf{s}_0 . Without loss of generality, we set the scattering plane $(\mathbf{s}, \mathbf{s}_0)$ as the x - o - z plane. The center position now is located at $\mathbf{r}^c = (r_x^c, 0, r_z^c)$. The orientations and lengths of the axes of the ellipsoid, which characterize the half-width of the spread of the distribution, can be computed as follows. The nonzero components for the second cumulant now are $(B_{xx}, B_{xz}, B_{zz}, B_{yy})$, expressed in Eq. (11). B_{yy} represents the length of one axis of the ellipsoid, perpendicular to the scattering plane. By diagonalizing the matrix

$$\begin{bmatrix} B_{xx} & B_{xz} \\ B_{xz} & B_{zz} \end{bmatrix}, \quad (48)$$

the lengths and directions of the other two axes of the ellipsoid on the scattering plane can be obtained. In fact, calculation shows that the direction of \mathbf{r}^c is also the direction of one axis of the ellipsoid, since at a certain time t the direction \mathbf{r}^c can replace \mathbf{s} as the unique special direction in the scattering plane. In order to reshape the distribution we choose a new \tilde{z} axis along the \mathbf{r}^c direction, and move the peak position of the distribution from $|\mathbf{r}^c|$ to z_c , taking this point as the origin of new coordinates $(\tilde{x}, \tilde{y}=y, \tilde{z})$, as shown schematically in Fig. 7.

In the new coordinates we use a shaped form similar to that of the 3D density Eqs. (42), while $\alpha(\tilde{\chi})$ in Eq. (42) is

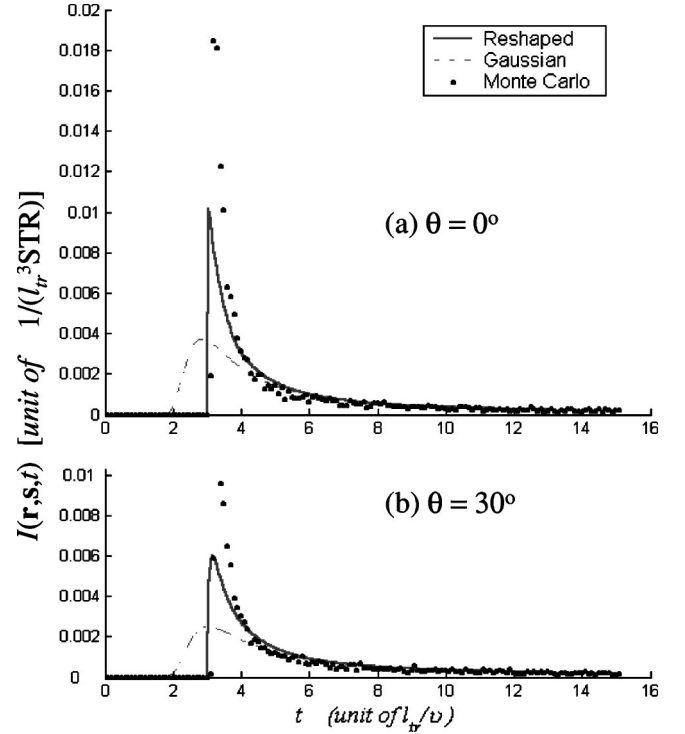


FIG. 8. Time-resolved profile of photon distribution function, for light directions $\theta =$ (a) 0° and (b) 30° , where the detector is located at $z = 3l_{tr}$ from the source along the incident direction, obtained by the reshaped form Eq. (42) (solid curves) and the Gaussian form (dashed curve), compared with that of the Monte Carlo simulation (dots). The Heyney-Greenstein phase function with $g = 0.9$ is used, and the absorption coefficient $1/l_a = 0$.

$$\begin{aligned} \alpha(\tilde{\chi}, \tilde{\varphi})^2 &\equiv \alpha_{\tilde{z}}^2 \cos^2(\tilde{\chi}) + \alpha_{\tilde{x}}^2 \sin^2(\tilde{\chi}) \cos^2(\tilde{\varphi}) \\ &+ \alpha_{\tilde{y}}^2 \sin^2(\tilde{\chi}) \sin^2(\tilde{\varphi}), \end{aligned} \quad (49)$$

where $\tilde{\chi}$ and $\tilde{\varphi}$ are, separately, the polar angle and the azimuthal angle of position $\tilde{\mathbf{r}}$ in the new coordinates. The parameters $(\alpha_{\tilde{x}}, \alpha_{\tilde{y}}, \alpha_{\tilde{z}}, z_c)$ are determined by fitting the center $|\mathbf{r}^c|$ and lengths of the three axes of the ellipsoid characterizing the half-width of the distribution. In many cases, the ellipsoid can be approximately treated as an ellipsoid of revolution; the length of the axis of the ellipsoid along the \tilde{x} direction is approximately equal to that along the \tilde{y} direction, and thus the computation can be simplified. The reshaped distribution function $I^{(s)}(\mathbf{r}, \mathbf{s}, t)$ for a certain direction \mathbf{s} is normalized to $F^{(s)}(\mathbf{s}, \mathbf{s}_0, t)$.

Figure 8 shows the computed time profile of the distribution function $I^{(s)}(\mathbf{r}, \mathbf{s}, t)$, when the detector is located at $3l_{tr}$ in front of the source, using the Heyney-Greenstein phase function with $g = 0.9$. Figures 8(a) and 8(b) are, separately, for different directions of light \mathbf{s} : $\theta = 0$ and 30° . The solid curves are for the reshaped form using Eq. (42) and the dashed curve is for the Gaussian form. The dots are for the Monte Carlo simulation. Anisotropic distribution is shown by comparing Figs. 8(a) and 8(b). The reshaped distribution removes intensity before $t_b = 3l_{tr}/v$, which appears in the Gaussian distribution. The reshaped distribution matches the Monte Carlo

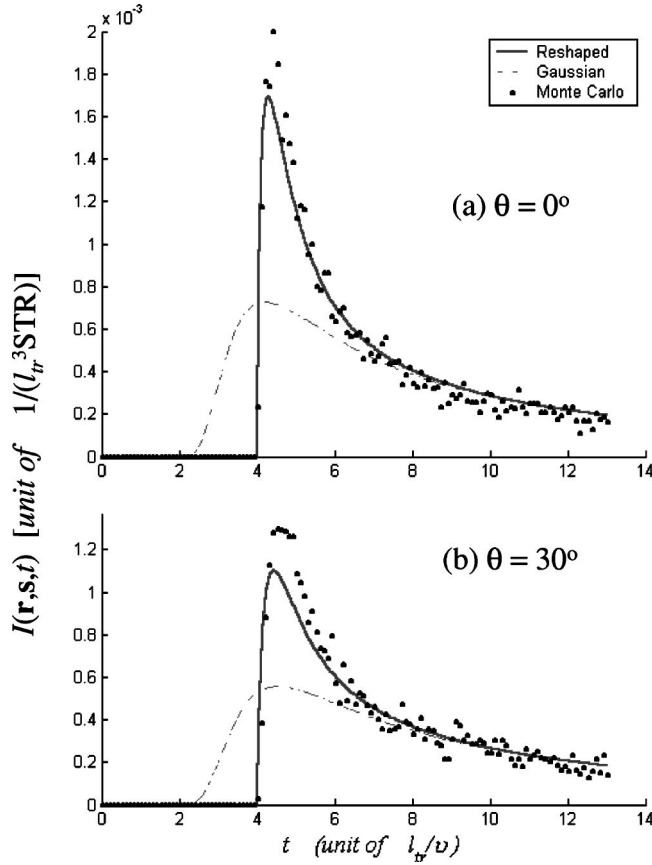


FIG. 9. Time-resolved profile of photon distribution function, for light directions $\theta =$ (a) 0° and (b) 30° , where the detector is located at $z = 4l_{tr}$ from the source along the incident direction. Other parameters are the same as in Fig. 8.

result much better than the Gaussian distribution, but the peak value is about 40% lower than that of the Monte Carlo simulation. Integrating over time shows that the difference in the steady state distribution function between the reshaped analytical model and the Monte Carlo simulation is about 7%. The ratio of the peak value at $\theta = 30^\circ$ is about 60% of that at $\theta = 0^\circ$, which shows stronger anisotropy at $d = 3l_{tr}$ compared to that at $d = 5l_{tr}$ shown in Fig. 2.

Figure 9 shows the distribution function $I^{(s)}(\mathbf{r}, \mathbf{s}, t)$ when the detector is located at $4l_{tr}$ in front of the source. The reshaped distribution matches the Monte Carlo result much better than that at $3l_{tr}$. It shows that the peak intensity at $4l_{tr}$ is about one order of magnitude smaller than that at $3l_{tr}$, but intensity decays with time more slowly at $4l_{tr}$ than at $3l_{tr}$.

V. DISCUSSION

While causality, together with the correct center and half-width of the distribution, are major controlling factors in determining the shape and the range of the particle distribution, the detailed shapes are, to some extent, different in the different models. Our choice of the reshaped form is based on simplicity and ease of computation, which obviously is not the only available choice. The initial results show that for $g = 0.9$ the parameters in our model can be quickly obtained

using the above fitting procedure up to $t \geq 4l_{tr}/v$ for the 3D case (up to $t \geq 2l_{tr}/v$ for 1D density). The Monte Carlo simulation is more time consuming in this time region. This model may work well for $g < 0.9$ in the above time region, because there is less forward scattering for a smaller g factor. The fitting error begins to increase during $3l_{tr}/v < t < 4l_{tr}/v$. At early time $t < 3l_{tr}/v$, \mathbf{r}^c becomes very close to the ballistic limit vt ; the front edge of the distribution almost perpendicularly jumps at the position vt . In this case, the parameter $z_c \approx vt$ in our model, is difficult to adjust through the fitting program. A more suitable model in this early time period is needed. Of course, Monte Carlo simulation also runs fast for short times and small spatial regions. For \mathbf{s} at the near backscattering direction, the Gaussian distribution can be a good approximation as shown in Fig. 3, because most particles suffer many scattering events to transfer from the forward direction to the backward direction. Our calculation shows that the center position \mathbf{r}^c is close to the source for $\theta \approx 180^\circ$ and far from the ballistic limit; hence, reshaping has little effect on the backscattering case.

In addition to improving convergence, separating the ballistic component from the scattered component also provides a more appropriate time-resolved profile for transmission. In the time-resolved transmission profile the ballistic component is described by a sharp jump exactly at time vt , separated from the later scattered component. The intensity of the ballistic component, compared to the scattered component, strongly depends on the g factor. For $g = 0$, $l_{tr} = l_s$, the ballistic component decays to $\exp(-1) = 0.368$ at distance $1l_{tr}$. But for $g = 0.9$ it decays to $\exp(-10) = 4.54 \times 10^{-5}$ at $1l_{tr}$, because $l_{tr} = 10l_s$. The jump of the ballistic component can be seen in experiments of transmission of light for a medium of small sized scatterers (small g factor), but is difficult to observe for a medium of large sized scatterers (large g factor). Our formula presented in Sec. III provides a good estimation for both small and large g factors by explicitly separating these two components.

Using the obtained analytical expressions, the distribution $I(\mathbf{r}, \mathbf{s}, t)$ can be computed very fast. The cumulant solution of the BTE has been extended to the case of a polarized photon distribution [11], and to semi-infinite and slab geometries [12]. Using a perturbation method, the distribution $I(\mathbf{r}, \mathbf{s}, t)$ in a weak heterogeneous medium can be calculated based on the cumulant solution of the BTE [12]. The nonlinear effect for strongly heterogeneous objects inside a medium can also be calculated using a correction of the “self-energy” diagram [13]. Hence, the analytical form of the solution of the BTE may have many different applications.

In summary, the analytical cumulant solution of the Boltzmann transport equation is improved in two respects. The ballistic component is separated and the cumulants for the scattered component are computed. This treatment ensures that summation-over l is convergent. We replace the Gaussian distribution by a different shaped form, which satisfies causality, and maintains the correct center position and the correct half-width of the distribution computed by our analytical formula. Our results show that the reshaped distribution matches that obtained by the Monte Carlo simulation much better than does the Gaussian distribution.

ACKNOWLEDGMENTS

This work was supported in part by NASA URC Center for Optical Sensing and Imaging at CCNY (NASA Grant No. NCC-1-03009), in part by the Office of Naval Research

(ONR), and in part by U.S. Army Medical Research and Materials Command. M.X. acknowledges support from the U.S. Department of the Army (Grant No. DAMD17-02-1-0516).

-
- [1] K. M. Case, P. F. Zweifel, *Linear Transport Theory* (Addison-Wesley, New York, 1967).
- [2] J. J. Duderstadt and W. R. Martin, *Transport Theory* (Wiley, New York, 1979).
- [3] S. Chandrasekhar, *Radiative Transfer* (Oxford University Press, New York, 1950).
- [4] P. Kubelka, *J. Opt. Soc. Am.* **44**, 330 (1954).
- [5] A. D. Kim and A. Ishimaru, *J. Comput. Phys.* **152**, 264 (1999).
- [6] L. Wang, S. L. Jacques, and L. Zheng, *Comput. Methods Programs Biomed.* **47**, 131 (1995).
- [7] W. Cai, M. Lax, and R. R. Alfano, *Phys. Rev. E* **61**, 3871 (2000).
- [8] W. Cai, M. Lax, and R. R. Alfano, *J. Phys. Chem. B* **104**, 3996 (2000).
- [9] M. E. Zevallos, A. Y. Polischuck, B. B. Das, F. Liu, and R. R. Alfano, *Phys. Rev. E* **57**, 7244 (1998).
- [10] R. F. Pawula, *Phys. Rev.* **162**, 186 (1967).
- [11] W. Cai, M. Lax, and R. R. Alfano, *Phys. Rev. E* **63**, 016606 (2000).
- [12] W. Cai, M. Xu, and R. R. Alfano, *IEEE J. Sel. Top. Quantum Electron.* **9**, 189 (2003).
- [13] M. Xu, W. Cai, and R. R. Alfano, *Opt. Lett.* **29**, 1757 (2004).